PAPER

Check for updates

Enhanced photoinduced antimicrobial properties of a copper(II) polypyridine naphthalene diimide complex for wound infection treatment and biomolecular interactions†

Leila Tabrizi,‡[a] Kaja Turzańska,‡[b] Ross McGarry,[a] Chloe Mullen,[a] John T. Costello, [iD][c] Deirdre Fitzgerald-Hughes [iD] *[b] and Mary T. Pryce [iD] *[a]

In this study, we synthesised and characterised a copper(II) naphthalenediimide-phenanthroline (NDI-Phen) compound and the corresponding copper complex. The photophysical properties of both the copper complex, $Cu(NDI\text{-}Phen)Cl_2$ (**Cu1**) and the *N*-octyl-*N*-[1,10]phenanthroline-1,4,5,8-naphthalenete-tracarboxylic-diimide (NDI-Phen, **L1**) were probed using laser flash photolysis on the nano to microsecond timescales. The biological properties of the **Cu1** complex and **L1** were evaluated based on their interactions with DNA, bovine serum albumin (BSA), and their antimicrobial properties against clinically important pathogens were determined. The binding affinity of the **Cu1** complex with calf thymus DNA (CT DNA) was evaluated using UV-Vis absorption titrations, and fluorescence quenching measurements. The results indicate a stronger intercalative binding mode for the copper complex, compared to **L1**, suggesting enhanced stabilisation with the DNA helix. The interaction with BSA was also studied for the **Cu1** complex, which exhibited a higher quenching and binding constant compared to **L1**. This suggests a stronger and more stable interaction with the protein, which may improve its bioavailability and resistance to degradation under physiological conditions. The **Cu1** complex demonstrated superior antibacterial activity when compared to **L1**. These findings suggest that complexation of the NDI-Phen unit with a copper centre significantly improves its potential as an antibacterial agent.

Introduction

Antimicrobial medicines are critical to human and animal health. They are used therapeutically in the management of infections and to support safer medical and surgical procedures, including cancer chemotherapy, organ transplant and insertion of in-dwelling medical devices. Antimicrobial resistance (AMR) is a natural evolutionary process among microorganisms, amplified by the widespread use and/or inappropriate use of antibiotics. AMR is among the top global threats to human health and the delivery of global healthcare.[1,2] While antimicrobial stewardship programs are implemented in many countries to preserve the efficacy of current antibiotics, investment in the antimicrobial pipeline is lacking. Relatively few new antibiotics have been approved for clinical use in recent years.[3] Most are derivatives of previously approved antibiotics and offer a short-term solution, since the resistance mechanisms against them are already established in nature.[4,5] Multidrug resistant bacteria that represent the gravest threats to patients in health care facilities are classified as priority pathogens by the World Health Organisation (WHO). The Infectious Disease Society of America (IDSA) coined the acronym ESKAPE (*Enterococcus faecium*, *Staphylococcus aureus*, *Klebsiella pneumoniae*, *Acinetobacter baumannii*, *Pseudomonas aeruginosa* and *Enterobacter* species) to encompass these pathogens.[6]

The AMR crisis results in increasingly limited antibiotics choices or reliance on more toxic or costly antibiotics, treatment failures, increased morbidity/mortality rates and significant costs. New drugs with entirely novel mechanisms of action to those currently available and with efficacy against ESKAPE pathogens should be a priority for novel antimicrobial development.[4,7]

Merging of expertise from inorganic chemistry and biology have resulted in the development of metal-based pharmaceuti-

[a]School of Chemical Sciences, Dublin City University, Dublin, D09W6Y4, Ireland. E-mail: mary.pryce@dcu.ie
[b]Clinical Microbiology, Royal College of Surgeons in Ireland, RCSI Education and Research, Beaumont Hospital, Beaumont, Dublin, D09YD60, Ireland. E-mail: dfitzgeraldhughes@rcsi.ie
[c]School of Physical Sciences, Dublin City University, Dublin 9, D09 K2WA, Ireland
†Electronic supplementary information (ESI) available. See DOI: https://doi.org/10.1039/d5dt01203a
‡Joint authors.

cals with transformative human health impacts in other areas of medicine, most notably cisplatin in cancer chemotherapy.[8] Among the transition metal complexes with antimicrobial properties, copper(II) complexes have been extensively studied. Copper is a bio-essential ion due to its redox nature and is responsible for several bioactivities in living organisms, such as enzymatic functions, electron transport, and redox signaling.[9–13] In addition to well-documented anticancer activity,[14–20] copper(II) complexes exhibit significant antimicrobial activities.[21–39] 1,10-Phenanthroline and its derivatives are a significant group of heterocyclics that act as chelating ligands in coordination chemistry and building blocks in supramolecular chemistry.[40] The photochemical and redox properties of heterocyclic complexes can be modified *via* suitable substitution on the phenanthroline rings.[41,42] Metal complexes of phenanthroline or modified phenanthroline ligands have potential in biological applications, with many having demonstrated DNA cleavage and antimicrobial activity.[43,44] The interaction of copper(II) complexes with DNA is another significant aspect of their biological activity. Copper complexes can bind to DNA through intercalation, groove binding, or electrostatic interactions, affecting the DNA structure and function. This binding can lead to DNA cleavage, which is central to anticancer therapies where DNA damage can induce cell death in rapidly dividing cancer cells.[45–47] Zelenko and colleagues (1997) synthesised Cu(phen)₂ and demonstrated its "chemical nuclease" activity. Cu(phen)₂ was proposed to partially bind to DNA *via* the intercalation of one phenanthroline ring.[48–50]

Metal-based complexes, including those of copper(II), have been reported to exhibit strong binding affinities to serum proteins such as bovine serum albumin (BSA).[45] These interactions can significantly influence their bioavailability, distribution, and elimination in biological systems. Understanding protein binding is therefore a key aspect in evaluating the pharmacokinetics and pharmacodynamics of metal-based therapeutic agents.[46,47]

Naphthalenediimide (NDI) derivatives are a class of π-electron-deficient, planar, and highly redox-active dyes that strongly absorb between 330–380 nm range. While their absorption in the near-UV region (∼350 nm) limits their utility in, *in vivo* diagnostic imaging—primarily due to poor tissue penetration and autofluorescence interference, recent developments have however demonstrated that NDI-based systems remain viable for therapeutic applications. In particular, the design of heavy-atom-free NDI-based donor–acceptor–donor structures has enabled dual-functional photodynamic and photothermal therapy (PDT–PTT), particularly under hypoxic tumor conditions where traditional oxygen-dependent PDT often fails. Min *et al.* (2025) demonstrated that NDI-based nanoparticles can effectively generate Type I ROS while also achieving high photothermal conversion efficiency (19.7%), thus offering a potent oxygen-independent therapeutic strategy.[51] Additionally, recent work has shown that core-extended NDI systems can act as selective, light-activated cytotoxic probes targeting tumor cells, and that related perylenediimide scaffolds are increasingly applied in phototherapy and bio-

imaging contexts.[52,53] These findings indicate that, although conventional diagnostic use may be constrained by optical properties, there are potential routes to developing therapeutic NDI-based platforms.

Recently, several NDI scaffolds were reported as anticancer agents, with properties of double stranded or G-quadruplex DNA binding, and reactive oxygen species (ROS) generation.[54–56] The nature and size of the side-chain terminal groups in NDI, which provide electrostatic interactions, are important factors in its binding selectivity.[55] Recently, Kuipers *et al.* reported the antibacterial activity of a Guanidine DNA quadruplex (G4-DNA) ligand library, based on the NDI pharmacophore, against both Gram-positive and Gram-negative bacteria.[57] Some platinum(II) diimine complexes of NDI are reported as electron-acceptor groups.[58,59]

In this study, we have synthesised a novel mononuclear copper(II) complex, designated as **Cu1**, comprising *N*-octyl-*N*-[1,10]phenanthroline-1,4,5,8-naphthalenetetracarboxylic-diimide. This innovative antimicrobial agent integrates a copper(II) centre, 1,10-phenanthroline, and photo-activated singlet oxygen, offering a unique approach to combating microbial infections. We investigated the photophysical properties, as well as the antibacterial efficacy of **Cu1** against representatives of ESKAPE pathogens. These pathogens included reference laboratory strains and clinical isolates, specifically those recovered from wound infections. Furthermore, we explored the photo-active antibacterial capabilities of **Cu1** when incorporated into a hydrogel matrix, aiming to enhance its practical application in medical treatments. Pluronic F127 is a hydrogel used for drug delivery in a range of therapeutic applications. It produces a transparent gel, useful for topical applications due to its biocompatibility and furthermore, it can be loaded with antibiotics or antimicrobial compounds. Although it has anti-adhesive properties, studies show that it has no intrinsic antimicrobial activity.[60] Incorporation of **Cu1** into the hydrogel not only demonstrated sustained antibacterial activity under light activation but also presented a viable method for localised treatment of infections. In addition to its antibacterial properties, we assessed the DNA/BSA-binding activity of the complex, which could further elucidate its mechanism of action at the molecular level. To the best of our knowledge, this is the first instance of designing a naphthalene-diimide copper complex tailored for biological applications. Our findings suggest that **Cu1** has potential to be used as a multifunctional agent in developing improved treatment strategies for wound infections and related conditions.

Experimental

Materials and instruments

All chemicals and solvents were obtained from Aldrich Chemicals Co. Anhydrous solvents with sure/seal were used under a nitrogen atmosphere. NMR spectra were recorded on a Bruker 600 MHz spectrometer and were referenced to the deuterated solvent peak as an internal reference. FT-IR spectra were obtained at room temperature using the Thermo

Scientific Nicolet iS5 IR-ATR instrument and Omnic Spectra software. The UV-Vis and emission spectra of **Cu1** and **L1** were recorded using a Horiba Duetta Fluorescence and Absorbance Spectrometer. All solutions were prepared in spectroscopy grade chloroform (Merck Life Science Ltd) using 1 cm quartz fluorescence cuvettes. Mass spectrometry was conducted using a Waters LCT Premiere XE mass spectrometer. Electron spray ionisation (ESI) (positive mode, Na$^+$) and a time of flight (TOF) mass analyser were employed. The samples were dissolved in a solution of 1% DMF in acetonitrile (ACN).

Time correlated single photon counting

Time correlated single photon counting (TCSPC) measurements were carried out using an FLS 1000 Photoluminescence spectrometer (Edinburgh Instruments) with a 375 nm diode laser. All samples were prepared to an absorbance of 0.3 at 375 nm, in a 1 cm quartz fluorescence cuvette. Lifetime measurements were obtained using both air equilibrated and N$_2$ purged samples. The UV-Vis spectra of the samples were compared, before and after the experiment to check for photostability. The analysis of the results was performed using Floracle® software.

Nanosecond transient absorption spectroscopy

Nanosecond transient absorption spectroscopy was performed using a LP980 transient absorption spectrometer (Edinburgh Instruments) with a Q-smart Q450 (Quantel) laser providing pulses with 3 mJ of energy at 355 nm. Samples were prepared by the Schlenk technique in speciality designed 1 cm fluorescence quartz cuvettes and measured under a N$_2$ environment. Similar to the TCSPC measurements, the optical density of the samples was ~0.3 at 355 nm. The UV-Vis spectrum of the samples was compared, before and after the experiment to check for the presence of photodegradation. The analysis of the results was performed using L900® software.

Synthesis

Synthesis of *N*-octyl-*N*-[1,10]phenanthroline-1,4,5,8-naphtha-lenetetracarboxylic-diimide (L1). **L1** was prepared according to literature procedures.[58,59] ^{1}H NMR (CDCl$_3$, 600 MHz) δ = 9.14–9.24 (m, 2H), 8.79 (s, 4H), 8.23–8.25 (m, 1H), 7.92–7.94 (m, 1H), 7.84 (s, 1H), 7.64–7.66 (m, 1H), 7.52–7.54 (m, 1H), 4.17 (t, *J* 7.68, 2H), 1.66–1.74 (m, 2H), 1.48 (s, 10H), 0.82 (t, t, *J* 6.84, 2H). ^{13}C NMR (CDCl$_3$): δ = 162.2, 158.8, 133.2, 131.2, 128.8, 127.9, 126.8, 122.7, 41.2, 31.8, 30.9, 29.3, 29.1, 27.0, 22.6, 14.1. FT-IR (ATR): ν 3076 (w), 2954 (w), 2922 (w), 2850 (w), 1708 (m), 1660 (s), 1580 (m), 1509 (w), 1450 (w), 1421 (w), 1371 (w), 1340 (s), 1242 (s), 1190 (m), 1133 (w), 1088 (m), 1017 (w), 974 (w), 886 (w), 804 (m), 767 (s), 737 (s), 700 (w), 625 (w), 561 (w), 461 (w), 405 (m) cm^{-1}. TOF-MS: *m/z*: 579.1980 [M + Na]$^+$. Anal. calc. (%) for C$_{34}$H$_{28}$N$_4$O$_4$: C, 73.37; H, 5.07; N, 10.07; found (%): C, 73.34; H, 5.08; N, 10.04.

Synthesis of (*N*-octyl-*N*-[1,10]phenanthroline-1,4,5,8-naphtha-lene-tetracarboxylic-diimide)-dichloro copper(II) (complex Cu1). A solution of 2 mL of DMF and CuCl$_2$·2H$_2$O (17 mg, 0.1 mmol) was added dropwise to **L1** (56 mg, 0.1 mmol) in 2 mL DMF and stirred at 70 °C for 24 hours. An immediate colour change

to deep blue was observed. The complex **Cu1** was precipitated by the addition of diethyl ether (50 mL) and a centrifuge. Yield (0.066 g, 95%). MS-TOF: 712.0684 [M + Na]$^+$. FT-IR: ν 3065 (w), 3012 (w), 2926 (w), 2861 (w), 1654 (s), 1517 (w), 1491 (m), 1464 (m), 1433 (m), 1385 (m), 1343 (w), 1317 (w), 1282 (w), 1253 (m), 1189 (w), 1091 (s), 983 (w), 906 (w), 862 (m), 821 (m), 798 (m), 765 (w), 721 (s), 658 (s), 544 (w), 512 (w), 479 (w), 426 (w) cm^{-1}. Anal. calc. (%) for C$_{34}$H$_{28}$Cl$_2$CuN$_4$O$_4$: C, 59.09; H, 4.08; N, 8.11; found (%): C, 59.06; H, 4.07; N, 8.08.

Solution stability study

The stability of the free ligand **L1** and complex **Cu1** were evaluated in Tris–HCl/NaCl, buffer solution containing 5% DMSO by monitoring them over 24 h at 37 °C using UV-Vis absorption spectroscopy (Fig. S8†). No change was observed in the absorption peaks of the UV-Vis spectra over this time, confirming that these compounds are stable under *in vitro* conditions.

DNA binding studies

DNA binding studies were carried out with CT DNA in 10 mM Tris–HCl/10 mM NaCl, buffer solutions, pH = 7.2. The quality/purity of the DNA stock solutions was assessed by determining the ratio of A_{260}/A_{280} which was ≥1.80. Stock solutions of DNA were stored at 4 °C in the dark and used within four days. The bulk DNA solution was further diluted 1/10 and showed a maximum absorbance at 260 nm. The absorption coefficient of CT DNA was 6600 cm^{-1} M^{-1} per nucleotide.[61] Solutions of compounds **L1**, **Cu1** (15 µM) in Tris–HCl/NaCl were prepared. Aliquots of the complex solutions were transferred to a cuvette containing DNA over the range 2–25 µM and changes in absorbance were measured.

The binding constant of the complexes with CT DNA (K_b) were obtained from the ratio of the slope to intercept in plots [DNA]/($\varepsilon_a - \varepsilon_f$) *versus* [DNA] according to the equation:[62]

$$[\text{DNA}]/(\varepsilon_a - \varepsilon_f) = [\text{DNA}]/(\varepsilon_b - \varepsilon_f) + 1/K_b\,(\varepsilon_b - \varepsilon_f)$$

where ε_a, corresponds to A_{obsd} for the Cu complex or ligand, ε_f represents the extinction coefficient for the free copper complex or ligand, and ε_b the extinction coefficient for the copper complex or ligand in the fully bound form.

Fluorescence spectroscopy, with ethidium bromide (EB) staining was used to investigate the binding of each complex to DNA. The EB solution was prepared in Tris–HCl/NaCl buffer (pH 7.2). Aliquots of 0–30 µM test solutions were added to DNA–EB (5 µM). The resulting solution was allowed to equilibrate for 2–5 min at room temperature. Changes in the fluorescence intensity at 620 nm (450 nm excitation) were recorded. The observed linearity in the plot of I_0/I *vs.* the concentration ratio of the compounds to DNA is in good agreement with the linear Stern–Volmer equation:[63]

$$I_0/I = 1 + K_{SV}\,[Q] \tag{1}$$

where, I_0 and I are the fluorescence intensities exhibited in the absence and presence of the compounds, respectively; [Q] corresponds to the concentration ratio of the compound to DNA.

Protein binding studies

The interaction of **L1** and **Cu1** with bovine serum albumin (BSA) was examined using fluorescence spectroscopy recorded at a fixed excitation wavelength of 280 nm (corresponding to BSA absorption) and monitoring the emission at 335 nm at 298 K. Throughout all experiments, the excitation and emission slit widths and scan rates were kept constant. UV–Vis absorption spectra were measured in the range of 200–800 nm at 298 K. A stock solution of BSA was prepared in a 50 mM phosphate buffer (pH 7.2) and stored in the dark at 4 °C for future use. Concentrated stock solutions of each test compound were prepared by dissolving the compound in phosphate buffer and then diluting with phosphate buffer to the required concentrations. A 2.5 mL solution containing BSA (10 μM) was titrated by successive additions of 0–24 μM test solutions (**L1** or **Cu1**) for fluorescence or UV-Vis measurements.

For a static quenching interaction, the fluorescence intensity data can also be used to determine the apparent binding constant (K_b) and the number of BSA binding sites (n) for the complex using the following equation:[64]

$$\log((I_0 - I)/I) = \log K_b + n \log [Q] \tag{2}$$

Procedure of singlet oxygen photogeneration

The procedure for singlet oxygen photogeneration was performed as described previously.[65,66] Aliquots (1.5 mL) of the compounds (5 μM) in methanol were added to 1.5 mL of 1,3-diphenylisobenzofuran (DPBF) (25 μM) in methanol in a quartz cell. Samples were irradiated using a 430 nm LED light source. The samples were placed in a 1 cm path length quartz cuvette and irradiated for up to 360 seconds. The distance from the LED source to the sample surface was maintained at 30 cm. Absorbance changes were recorded at fixed intervals using a UV–vis spectrophotometer. The absorption intensity of DPBF at 410 nm was used to estimate the quantum yields for the generation of singlet oxygen. The formula for estimating the singlet oxygen quantum yield (Φ) was adapted from the following equation:

$$\Phi_S = \Phi_{Ref} \cdot (m_s/m_{Ref}) \cdot (\alpha_{Ref}/\alpha_s) \tag{3}$$

where the indexes s and Ref indicate investigated compounds and Rose Bengal, respectively, Φ is the quantum yield of singlet oxygen photogeneration; m is the slope of a trend line of change in the absorbance of DPBF (at 410 nm) *vs.* time and α is the absorption correction factor given by $\alpha = 1-10^{-A}$ (A is the absorbance at 430 nm).

Antimicrobial testing

Strains and isolates. Light-activated bactericidal activity of compounds was investigated against reference strains of *Escherichia coli* (ATCC 25922), *Staphylococcus aureus* (ATCC 25923) and *Pseudomonas aeruginosa* (ATCC 27853) initially, to establish time and concentration dependence. Thereafter, further reference strains representing WHO designated priority pathogens (ESKAPE) were included to establish the spectrum

of activity. Reference strains were sourced from the American Tissue Culture Collection (ATCC) or the National Collection of Type Cultures (NCTC), United Kingdom Health Security Agency (UK HSA). Where possible, an AMR strain and an anti-biotic susceptible strain was included. In addition, clinical isolates recovered from wound infections were investigated. These were provided anonymously following confirmation of their identity to species level by Matrix Assisted Laser Ionisation Desorption Time of Flight Mass Spectrometry (MALDI-TOF MS) using a Brüker Daltonik MALDI Biotyper. Ethical approval was obtained from Beaumont Hospital Ethics Committee (reference number 22/17) for use of these isolates. No patient information was collected. Details of the strains and isolates used are described in detail in a previous publication by Doherty *et al.*[67]

Bactericidal assay

Compounds were prepared as 1 mg ml^{-1} stocks in phosphate buffered saline (PBS) containing 10% DMSO and further diluted as required. Bacterial colonies were plated onto Mueller–Hinton (MH) agar and grown aerobically at 37 °C overnight in a static incubator (Pol-Eko Aparatura). A bacterial suspension was prepared from single colonies using PBS to a density of 0.5 McFarland using a pre-calibrated turbidometer (Densichek™, Biomerieux). The suspension was further diluted 1/1000 in PBS (between 10^5–10^6 colony forming units (CFU) per ml approx.). Assays were prepared in triplicate, in 96 well plates by adding 20 μl of stock solution to 180 μl of diluted bacterial suspension. Two control series were prepared in which test compounds were replaced by diluent (PBS) or 10% DMSO. Where irradiation was required, duplicate plates were prepared in this way, one was irradiated with a LED light source (dichromatic lamp, λ_{exc} = 430 and 660 nm) suspended at 30 cm above the plate, for up to 1 h at room temperature. The fluence rate (21.93 mW cm^{-2}) at this distance was measured using a radiometer (Delta Ohm HD 2101.2) equipped with an irradiance probe (LP 471 RAD). The temperature was monitored during irradiation. The second 96-well plate was incubated in the dark at room temperature for the same time period. The Miles *et al.*, method was used to enumerate the bacteria.[68] Briefly, after irradiation/incubation, 1/10 serial dilutions were prepared (10^{-1} to 10^{-4}) from treated and control wells under light and dark conditions, in PBS. Aliquots (20 μL) from these dilutions were applied in triplicate to four quadrants of MH agar plates. The plates were incubated overnight at 37 °C in a static incubator. Resulting colonies were counted, and bactericidal activity for light and dark conditions, was determined based on log$_{10}$ reduction in CFU mL^{-1} compared to untreated negative controls.

Antimicrobial testing of Cu1 incorporated in a hydrogel

Pluronic F127, 18% (w/v) in deionized water was prepared by vigorous stirring at 4 °C for 24 h to obtain a clear solution, which was then filtered (0.22 mm filter, Millipore). Aliquots (900 μl) were prepared containing 100 μl of compound dissolved in DMSO or DMSO alone as a control. Bacterial suspen-

sions (100 μl), prepared as described earlier, were added to 96-well plates, followed by 100 μl of Pluronic F127-containing test compound/DMSO. Duplicate plates were prepared in this way, one was irradiated as described above, the second was incubated in the dark at room temperature. The Miles *et al.* method was used to enumerate bacteria, as described above.

Biocompatibility investigations

Potential cytotoxicity to human cells was investigated by determining metabolic activity in keratinocytes in culture and haemolytic activity in primary human erythrocytes. As described previously,[69] human HaCaT cells (aneuploid immortal keratinocyte cell line) were cultured in Dulbecco's modified Eagle's medium (Gibco) supplemented with 10% foetal bovine serum. Cells were seeded at 3×10^5 cells per mL for 24 hours at 37 °C, before incubation with doubling dilutions of **Cu1** and **L1** from 800 to 1.56 μg ml^{-1} in a final volume of 10% DMSO (v/v) for 24 h in dark conditions only (light conditions were not investigated, in this case as this required removal of the plates from CO_2 incubator for prolonged periods and resulted in cell detachment due to their high pH sensitivity in this condition). Triton-X-100 (2%, v/v) was used as a positive control and culture media alone as a negative control. Media were removed, and the cells were washed and incubated with 100 μL of 500 mg L^{-1} MTT (3-[4,5-dimethyl-2-thiazolyl]-2,5-diphenyl-2*H*-tetrazolium bromide; Sigma) for 4 hours, protected from light. DMSO was added to solubilise, and plates were covered with aluminium foil and agitated on an orbital shaker for 5–10 min. The absorbance was read at 590/595 nm using a plate reader (VICTOR™ X3 2030 Multilabel Reader,

PerkinElmer). For estimation of haemolysis, the method described by Zapotoczna *et al.* was used.[69] Briefly, healthy human volunteer blood was drawn into tubes containing EDTA; 1.6 mg mL^{-1}. Erythrocytes were separated by centrifugation at 1000g for 5 min at 18 °C and were washed twice with PBS. The washed pellet was resuspended to five times the original volume of blood collected. In a 96 well plate, 50 μL of the erythrocyte suspension was mixed with 50 μl of **Cu1** and **L1** in 10% DMSO. Positive control (100% haemolysis) contained Triton-X-100 (2%, v/v) and negative controls (0% haemolysis) contained PBS instead of compounds. After 24 h of incubation at 37 °C, the plates were centrifuged for 5 min at 500g. The supernatant was removed into new 96 well-plates and the absorbance was measured with a plate reader (VICTOR™ X3 2030 Multilabel Reader, PerkinElmer) at a wavelength of 405 nm. For both biocompatibility assays, retention of metabolic activity (MTT assay) and % haemolysis was estimated with reference to controls. Ethical approval with explicit consent for human volunteer blood was obtained from the Royal College of Surgeons Research Ethics Committee, reference number 202203014.

Results and discussion

Synthesis and characterisation

The *N*-octyl-*N*-[1,10]phenanthroline-1,4,5,8-naphthalenetetra-carboxylic-diimide (**L1**) ligand was prepared according to a literature procedure.[59] Subsequent treatment of **L1** by CuCl$_2$·2H$_2$O in DMF generated the **Cu1** complex (Fig. 1). The
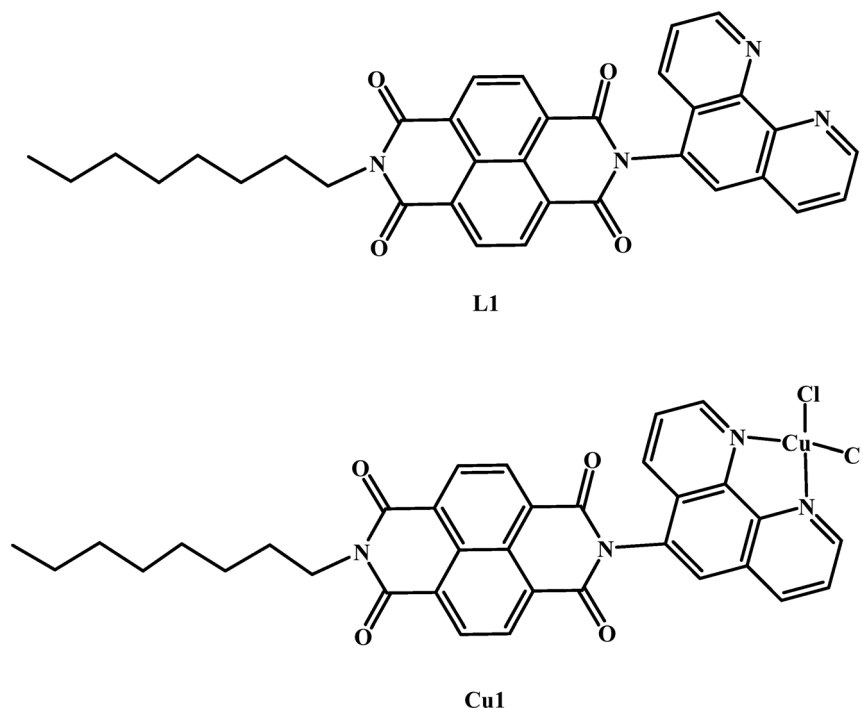

L1

Cu1

Fig. 1 The structures of ligand **L1** and complex **Cu1**.

L1 ligand was characterised by ^{1}H and ^{13}C NMR spectroscopy (Fig. S1 and S2†). The ESI-MS spectra show peaks centered at m/z 579.1980 ± 4.9 ppm for **L1** ([M + Na]$^+$) and at m/z 712.0684 ± 0.4 ppm for **Cu1** ([M + Na]$^+$). The observed peaks are consistent with simulated isotopic patterns (Fig. S3 and S4†). The IR spectra for the ligand **L1** and the complex **Cu1** (Fig. S5 and S6†) display stretching bands consistent with the proposed structures. The stretching vibrations of the imide groups in the range 1710–1650 cm^{-1} (ν(C=O)) in both **Cu1** and **L1** overlap when ATR (attenuated total reflectance) is used.

Time resolved photophysical measurements

The UV-Vis spectrum of **L1**, is displayed in Fig. 2a. Three characteristic absorption peaks are observed at 383, 340 and 302 nm, arising from S_0–S_1 (π–π^*) transitions of the naphthalene diimide core,[70,71] with π–π^* transitions observed at 267 nm. The compound features an emission band with a maximum at 393 nm that is assigned to the S_1–S_0 relaxation, with significant tailing to 700 nm, indicative of the formation of excimers.[72] The same phenomenon has been observed in other NDI systems and related compounds.[71,73] The UV-Vis spectrum of the **Cu1** complex is broadly similar to that of **L1** with a slight redshift (Fig. 2b), and absorption features between 260–400 nm assigned to π–π^* transitions.[70,74] Furthermore, weak d–d transitions are observed between 400–540 nm. Unlike **L1** the copper complex displayed no emission in the visible region.

Transient absorption spectroscopy was carried out on both **L1** and **Cu1** and the results are displayed in Fig. 3 and 4 respectively. The changes in the transient absorption spectra are indicated by the black arrows. **L1** displayed ground state bleaches at 380 nm and excited state absorption features were observed between 395 nm to 550 nm, which closely matches the spectral signatures of the ^{3}NDI (Fig. 3) species.[75,76] The kinetic profile of the parent bleach was recorded at 380 nm and displayed two long-lived lifetimes of 33 μs and 122 μs respectively. These lifetimes were assigned to a naphthalene diimide centred triplet state and its biexponential behaviour was attributed to self-quenching of the molecule.[72,77] Due to the planar nature of the compound, these systems regularly aggregate.[72,73] This resulting aggregation, at higher concentrations and laser energy, typically results in self-quenching of the system via triplet–triplet annihilation.

The transient absorption spectrum of **Cu1** following excitation at 355 nm (Fig. 4) is similar to that obtained for **L1**, with ground state bleaching at 380 nm and excited state absorptions observed between 395 nm to 550 nm. As for **L1**, the ESA features are assigned to ^{3}NDI.[75,76] The kinetic profile of **Cu1** at 480 nm and was fitted with a mono-exponential curve yielding a lifetime of 270 ns. Based on the observed spectral signals, this lifetime was assigned to a ^{3}NDI state and its subsequent recovery to the ground state.

Singlet oxygen (^{1}O$_2$) production measurements

Singlet oxygen detection, generated from **L1** and **Cu1** was carried out by monitoring the change in absorbance of DFBF at 410 nm during different irradiation times using a 395 nm LED (Fig. S7†). The irradiated solutions contain air-saturated solutions of DPBF in methanol with **L1** or **Cu1**. Fig. S7†-insert is obtained by plotting A/A_0 versus time, where A is the absorbance at 410 nm in the presence of **L1** or **Cu1**, and A_0 is the initial absorbance. The quantum yields of singlet oxygen (Φ_Δ) for **L1** and **Cu1** were 0.73 and 0.30, respectively. The quantum yield of singlet oxygen (Φ_Δ) for Rose Bengal as a reference was 0.80 according to a report in the literature.[65]

The generation of singlet oxygen by **Cu1** indicates the involvement of an excited triplet state, which is consistent with the transient absorption spectroscopy data. The observed spectral features and the kinetic lifetime of 270 ns strongly support the formation of a ^{3}NDI triplet state. Although the lifetime is significantly shorter than that of the free ligand **L1**, it remains sufficiently long to enable energy transfer to ground-state molecular oxygen, thereby producing singlet oxygen with a Φ_Δ of 0.30. This demonstrates that **Cu1** undergoes intersystem crossing to a triplet state, which serves as the reactive intermediate in the generation of singlet oxygen.

DNA binding studies

UV–Vis absorption spectroscopy. Electronic absorption spectroscopy is widely used to assess the binding of complexes with DNA. Typically, a red shift (or blue shift) and a hypochromic (or hyperchromic) effect are observed in the absorption spectra of small molecules when they intercalate with DNA. With increasing CT DNA (0–25 μM), the π–π^* absorption bands of **L1** and **Cu1** exhibit a hypochromism with a red shift of ~3 nm for **L1** and 7 nm for **Cu1**. While the broad bands in the range 325 to 395 nm (corresponding to the n–π^* transition in **L1** and ^{1}MLCT (d–π^*) in **Cu1**) remain unshifted in the UV-Vis spectra for **L1** and **Cu1** (Fig. 5 and S9†). Successive addition of DNA to either **L1** and **Cu1** aliquots, induce a slight red shift attributed to intercalation and strong stacking interactions between the aromatic chromophore and the base pairs of DNA.[78–80] A plot of [DNA]/(ε_a – ε_f) versus [DNA] gives a slope of $1/(\varepsilon_b – \varepsilon_f)$ and a y-intercept equal to $1/K_b$ ($\varepsilon_b – \varepsilon_f$); K_b is the ratio of the slope to the y-intercept (Fig. 5 and S10†). The binding constants (K_b) obtained for **L1** and **Cu1** are (1.51 ± 0.02) × 10^4 M^{-1}, and (3.69 ± 0.02) × 10^5 M^{-1}, respectively. The increase in K_b for **Cu1** indicates a strong binding affinity for CT DNA compared to **L1**.

To assess the relative strength of these interactions, the DNA-binding behavior of ethidium bromide (EtBr), a well-known DNA intercalator, was also evaluated (Fig. S10†). EtBr exhibits hypochromism with a red shift of ~3 nm upon binding to CT DNA, with a binding constant of (1.20 ± 0.02) × 10^5 M^{-1}. There is a threefold increase in the binding constant of **Cu1** with CT DNA compared to that with EtBr. In the case of **L1**, the binding with CT DNA is significantly less than with EtBr (1.51 ± 0.02) × 10^4 M^{-1} vs. (1.20 ± 0.02) × 10^5 M^{-1}.

The significantly higher DNA-binding affinity of **Cu1** compared to **L1** can be attributed primarily to the coordination of the copper(ɪɪ) ion and its influence on the molecular geometry and electronic properties of the complex. Although both com-
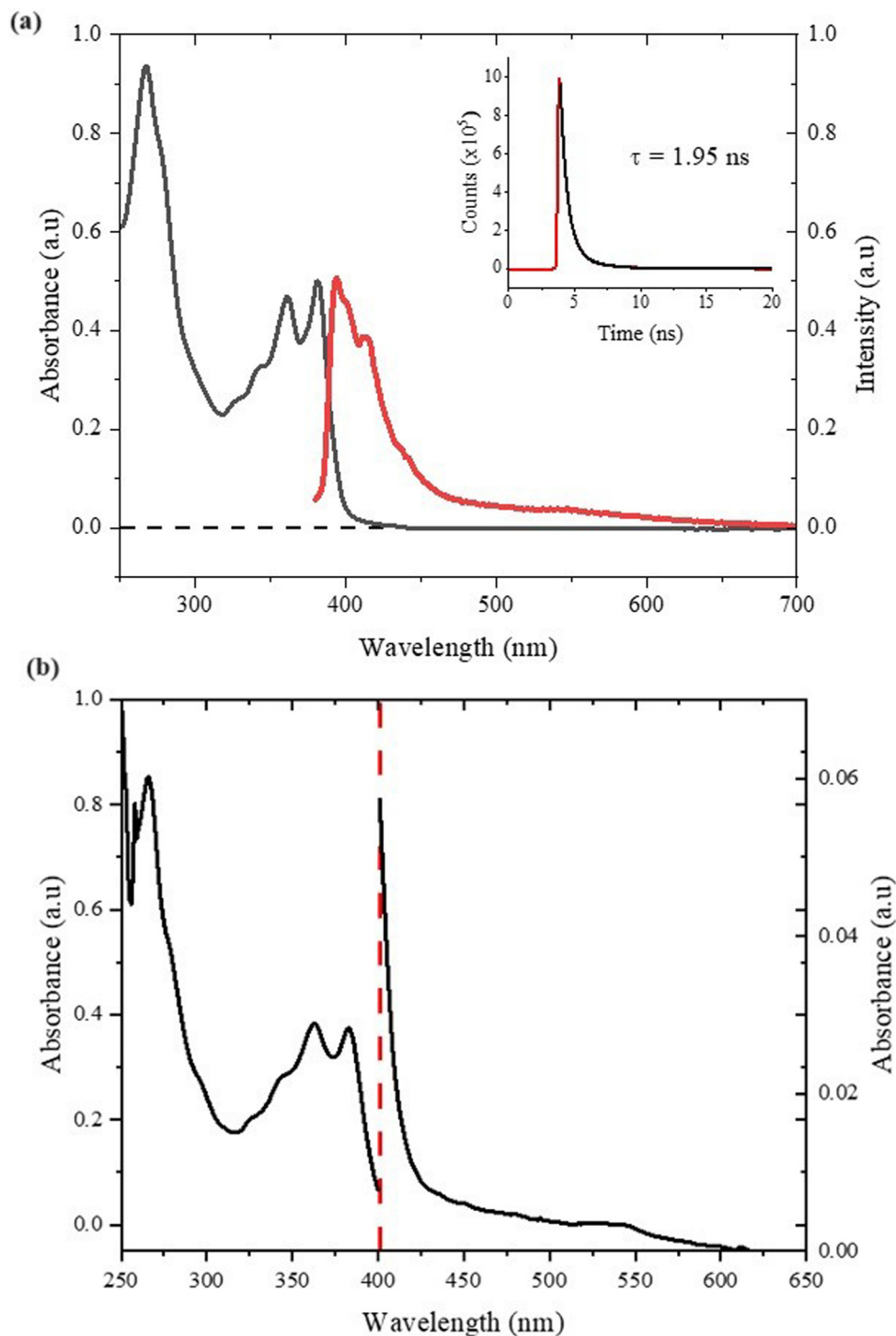
Fig. 2 (a) The normalised UV-Vis and emission spectra of **L1**. The insert displays the emission lifetime of **L1**, recorded at 393 nm, following excitation at 375 nm. (b) The UV-Vis spectrum of **Cu1**. All spectra were recorded in chloroform.

pounds contain the NDI moiety, which contributes to π–π stacking interactions with DNA base pairs, and incorporation of Cu(II) may result in electrostatic interactions with the negatively charged phosphate backbone of DNA, further stabilizing the complex DNA association. These combined effects, absent in the free ligand **L1**, may account for the substantially higher binding constant observed for **Cu1**.[48,49,54,55]

The binding constant of **Cu1** with DNA was found to be substantially higher than that of previously reported-phenanthroline copper(II) complexes with binding constants of 2.82 ×

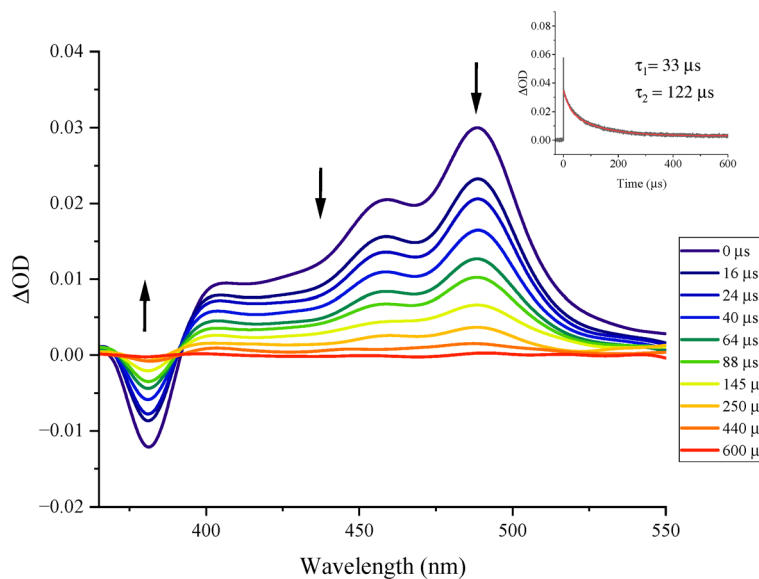**Fig. 3** The transient absorption spectra of **L1** in CHCl$_3$ (λ_{ex} = 355 nm), recorded over a 600 µs time range. The insert displays the kinetic trace recorded at 380 nm.
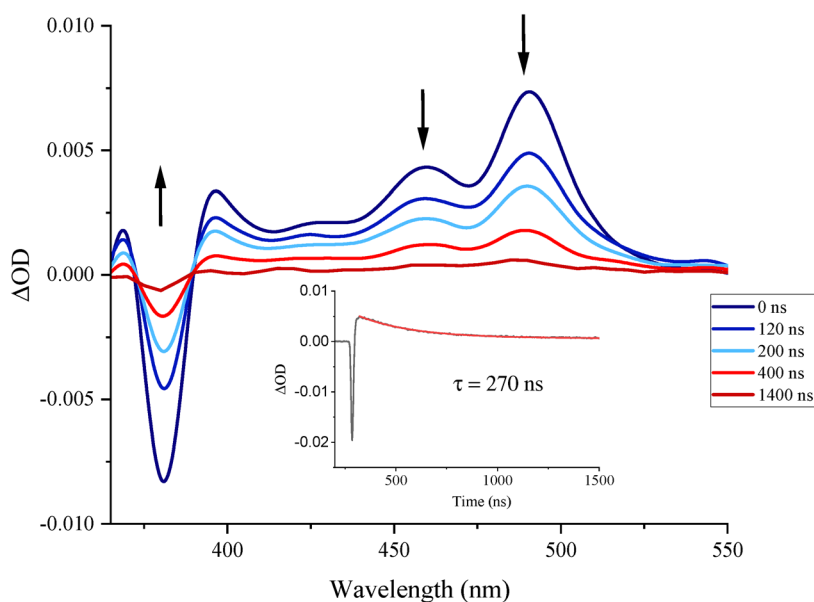

Fig. 4 The transient absorption spectrum of **Cu1** in CHCl$_3$ (λ_{ex} = 355 nm), recorded over a 1400 ns time range. The insert displays the kinetic trace recorded at 380 nm.

10^4 M^{-1} or 1.05 × 10^3 M^{-1} reported.[81,82] The higher value of 3.69 × 10^5 M^{-1}, observed by us, is attributed to π–π stacking interactions as a result of the naphthalenediimide moiety. The aromatic structure of naphthalenediimide facilitates stronger intercalation between the DNA base pairs, thereby increasing the stability of the Cu complex–DNA interaction.[83,84]

Ethidium bromide–DNA fluorescence quenching. To further confirm the interaction mode, the binding of **L1** and **Cu1** to CT DNA was studied through a competitive binding fluorescence assay using ethidium bromide (EB). In our experiments, the addition of various amounts of **L1** and **Cu1** to DNA pre-treated with EB resulted in a significant reduction in fluorescence emission intensity (Fig. 6 and S11†). This reduction is due to the replacement of the EB fluorophore in the EB–DNA adduct by the complex, leading to a corresponding decrease in emission intensity suggesting that intercalation occurs between **Cu1** and DNA.[85] The slope of the plot of I_0/I versus [Q] gives K_{SV} (Fig. 6 and S11†). The Stern–Volmer constant, K_{SV}, was calculated to be (3.68 ± 0.02) × 10^4 M^{-1} for **L1** and (6.53 ± 0.02) × 10^4 M^{-1} for **Cu1**.

Fig. 5 UV-Vis absorption spectra of **Cu1** in Tris-HCl buffer upon the addition of CT DNA. [**Cu1**] = 15 μM, [DNA] = 0–25 μM. The absorption decreases upon increasing DNA concentration. Insert: Plot of [DNA]/(ε_a − -ε_f) versus [DNA] for the titration of **Cu1** with CT DNA.
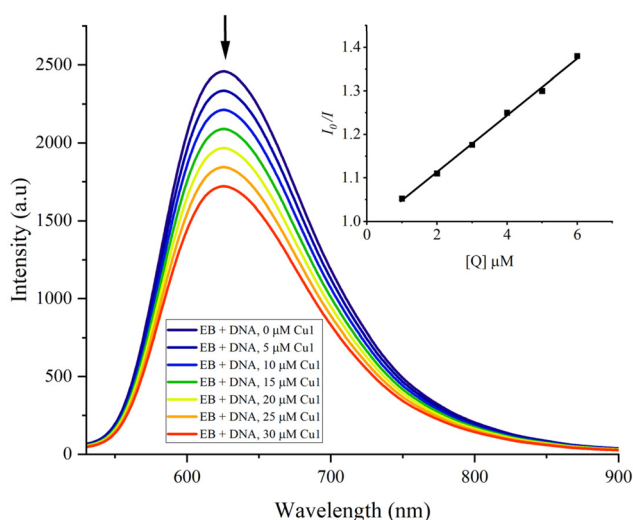

Fig. 6 Fluorescence quenching curves of EB bound to DNA in the presence of complex **Cu1** in Tris-HCl buffer. [DNA] = 5 μM, [EB] = 5 μM and [**Cu1**] = 0–30 μM. Insert: Stern–Volmer plot of fluorescence titrations of the complex **Cu1** with CT DNA.

The quenching constant (K_q) can be obtained from the equation, $K_{SV} = K_q\tau_0$, where τ_0 is the lifetime of the fluorophore (CT-DNA–EB) in the absence of the quencher (19.2 ns).[86] The K_q, was calculated to be $(1.92 \pm 0.02) \times 10^{12}$ M^{-1} S^{-1} for **L1** and $(3.4 \pm 0.02) \times 10^{12}$ M^{-1} S^{-1} for **Cu1**. The quenching constants obtained for both compounds, **L1** and **Cu1** are similar. While this assay provides no information on the binding mode, it does confirm the strength of the interaction.

Protein binding studies

BSA is a widely studied protein due to its structural homology with human serum albumin and its applications in drug delivery and biochemical research. Intercalation of ligands and complexes with BSA can reveal crucial information about binding modes, stability, and potential applications in pharmaceuticals.[87] Naphthalenediimide (NDI) derivatives are known for their strong π–π stacking interactions and electron-accepting properties.[88] Phenanthroline is another compound with significant binding capabilities.[89] When combined, these ligands can form interesting complexes with metals such as copper, thus enhancing their binding interactions and biological relevance.[89–91]

A simple method used to distinguish the protein-binding ability of drugs is UV–Vis absorption spectroscopy.[92,93] Displayed in Fig. 7 and S12† are the UV–Vis absorption spectra of BSA in the presence of various concentrations of **Cu1** and **L1**, respectively. Two types of quenching can occur, namely dynamic and static. Displayed in Fig. 7 and S12† are the changes in the absorption spectra of BSA and BSA-**Cu1** or **L1**. The absorption spectra of BSA exhibit a peak at 278 nm. Upon the addition of **L1**, no shift of the 278 nm peak occurs (Fig. S12†). However, with the addition of **Cu1**, the absorption decreases together with a red shift of 4 nm (Fig. S7†). This result is indicative of static quenching, with the formation of a new ground state complex of a BSA-**Cu1** type. In contrast, the interaction between **L1** and BSA does not lead to the formation of a ground state complex, suggesting a dynamic quenching process instead.

The interaction of **L1** and **Cu1** with BSA was investigated using fluorescence spectroscopy, an effective method for quali-
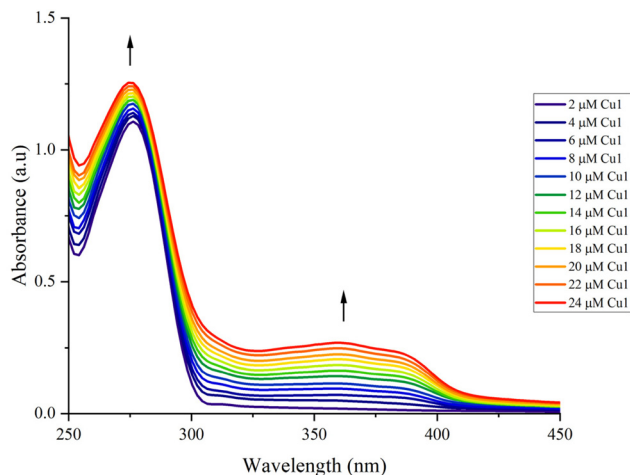
Fig. 7 UV-Vis absorption spectra of BSA (10 μM) in PBS solution in the presence of different amounts (0–24 μM) of **Cu1**.

tatively analysing the binding of complexes to BSA. The native fluorescence of BSA arises from three protein residues: tryptophan, tyrosine, and phenylalanine, with the fluorescence at 348 nm primarily attributable to tryptophan residues. Fluorescence quenching is indicative of BSA binding. Fig. 8 and S13† display the fluorescence emission spectra of BSA in the presence of different concentrations of **Cu1** and **L1**, respectively. For both compounds, there was no significant difference in the emission profile or emission wavelength, thereby indicating that the conformation of BSA did not change significantly. The emission intensity of BSA did however decrease upon the addition of **L1** or **Cu1**, suggesting that both compounds interact with BSA near the tryptophan residues.

The Stern–Volmer constant, K_{SV}, were calculated $(1.07 \pm 0.03) \times 10^5$ M^{-1} for **L1** and $(2.50 \pm 0.02) \times 10^5$ M^{-1} for **Cu1** (Fig. 8 and S13†). The quenching constants (K_q) were obtained

from the equation, $K_{SV} = K_q\tau_0$, where τ_0 is the lifetime of the fluorophore (BSA) in the absence of the quencher (10 ns).[94] The K_q value was calculated to be $(10.7 \pm 0.03) \times 10^{12}$ M^{-1} S^{-1} for **L1** and $(25 \pm 0.02) \times 10^{12}$ M^{-1} S^{-1} for **Cu1**. The K_q value for **Cu1** was higher than that for **L1**, and for both compounds, it was significantly higher than the proposed value of the order of 10^{10} M^{-1} s^{-1} for diffusion-controlled dynamic quenching. Therefore, it can be assumed that the interaction of **L1** and **Cu1** with BSA follows a static quenching process.[95]

From the plot of $\log((I_0 - I)/I)$ versus $\log[Q]$ (Fig. S14†), the number of binding sites (n) and the binding constant (K_b) values have been calculated. For both compounds, a linear relation is observed with comparable binding constant K_b of 8.86×10^6 and 9.29×10^6 for **L1** and **Cu1**, respectively. In both compounds, the value of n was calculated to be 1.15 and 1.13 for **L1** and **Cu1**, respectively. Both values are close to 1, suggesting that there is only one binding site for **L1** or **Cu1** on the BSA molecule. The BSA binding constant of the **Cu1** complex was of the order of 10^6 M^{-1} which indicates strong binding with BSA. Previous studies by others indicated that several copper complexes bind strongly to BSA with a binding constant ranging between 10^3 M^{-1} to 10^5 M^{-1}.[96–98] The higher binding affinity of **Cu1** to BSA compared to other copper complexes is attributed predominantly to π–π stacking interactions. The potential for π–π interactions between the aromatic rings of the naphthalenediimide and the aromatic amino acids within BSA further stabilises the interaction.[99–101] Future studies are required to gain a more detailed insight into the mechanism.

Antimicrobial activity under dark and light activation conditions

Initial evaluation of complexes was against *S. aureus* 25923, *E. coli* 25922 and *P. aeruginosa* 27853. In the absence of light activation, 24 h incubation with **Cu1** (100 μg ml^{-1}, 145.1 μM) resulted in 6 log reduction in CFU ml^{-1} for *S. aureus*, *E. coli* (which was the upper limit of the assay) and almost 2 log reduction for *P. aeruginosa*. In comparison **L1** had low or negligible activity under the same conditions, with 1.1, 0.6 and 0 log respectively (Fig. 9). The full range of ESKAPE pathogens, including antibiotic resistant strains was next tested. In the dark, 24 h incubation resulted in high level (5–6 log) killing for *S. aureus*, *E. coli* and *A. baumanii*, but less potent activity was found among other ESKAPE pathogens (Fig. 10). This pattern of activity is perhaps unsurprising given the known antimicrobial properties of copper. Indeed, the spectrum of activity of copper-1,10 phenanthroline complexes against healthcare-associated pathogens are reported to vary. Pereira *et al.* reported bacteristatic and bactericidal activity of a number of Cu(II)-1,10 phenathroline complexes by determining the minimum inhibitory concentration (MIC) and minimum bactericidal concentration (MBC) against *S. aureus* with MIC/ MBCs from 31.25 to 125 μg ml^{-1} but >500 μg ml^{-1} for *E. coli*.[102] In another study MICs of 5–25 μg ml^{-1} were reported for *S. aureus* and *K. pneumoniae* but poor susceptibility of *P. aeruginosa* to Cu(II)-1,10 phenanthroline complexes.[103]
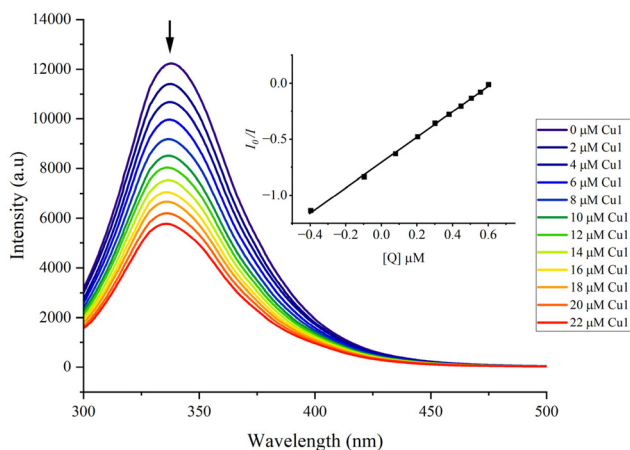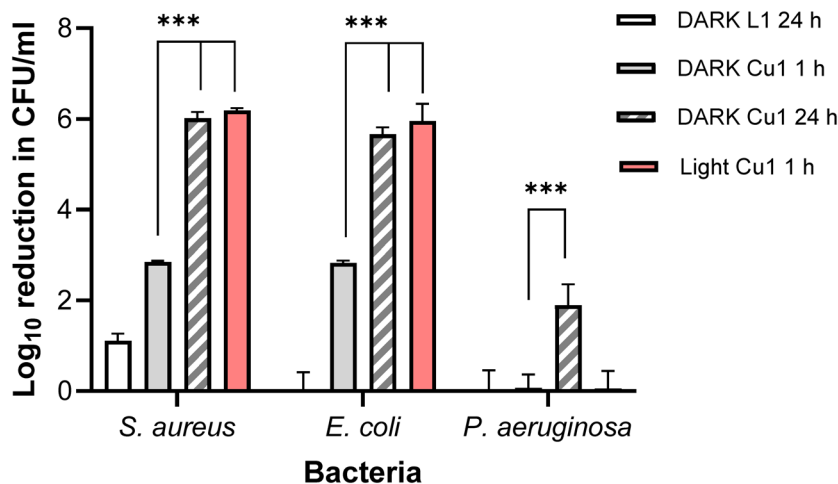

Fig. 8 Fluorescence quenching curves of BSA (10 μM) in PBS solution in the presence of different amounts (0–24 μM) of **Cu1**. Insert: Stern–Volmer plot of the fluorescence titrations.

Fig. 9 Bactericidal activity of **L1** and **Cu1** against *S. aureus* (ATCC 25923), *E. coli* (ATCC 25922), and *P. aeruginosa* (ATCC 27853). Approximately 10^6 CFUs of each bacteria were incubated for 24 h in the dark, with 100 μg ml^{-1} compounds (179.8 μM **L1**, 145.1 μM **Cu1**). In controls, compounds were replaced with 10% DMSO. Values are presented as log reduction in CFU ml^{-1} with respect to controls. Data are the mean ± SEM for 3 experiments. Statistically significant values are indicated, *** = $P \leq 0.001$ (two-way ANOVA).
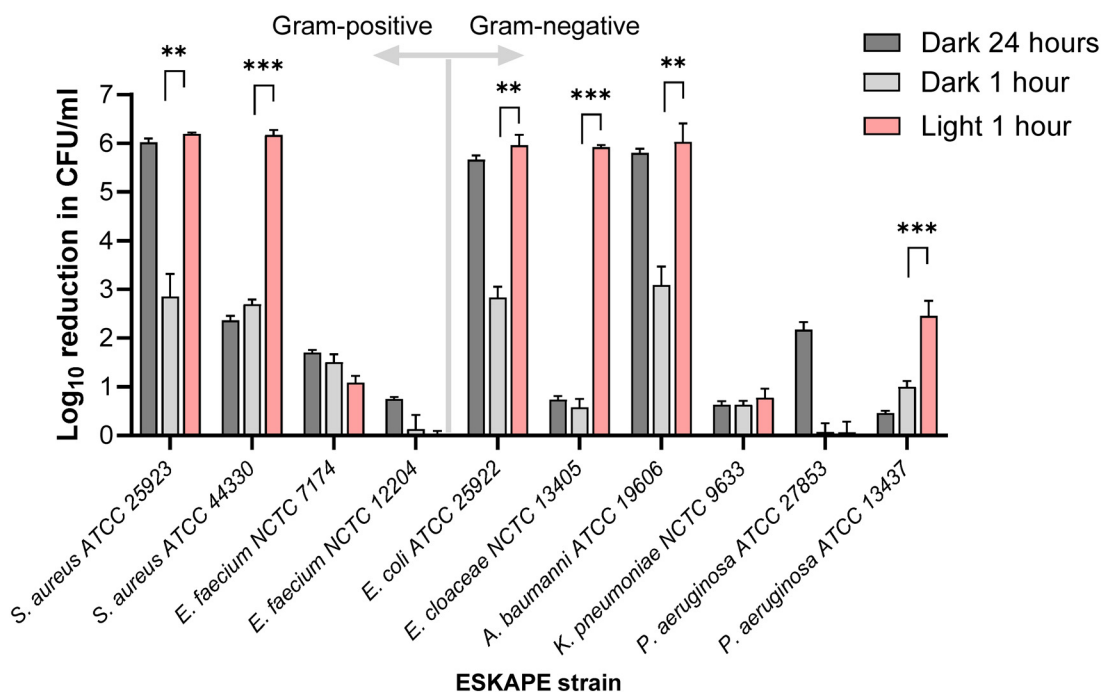

Fig. 10 Bactericidal activity of **Cu1** against ESKAPE reference strains. Approximately 10^6 CFU ml^{-1} of each bacteria were incubated in the dark (grey bars, 24 h or 1 h) and with light irradiation (pink bars) at 430 nm for 1 h. Values are log reduction in CFU ml^{-1} with respect to growth controls (bacteria incubated without 10% DMSO instead of 100 μg ml^{-1} **Cu1**). Data are the mean ± SEM for 3 experiments. Statistically significant differences between light and dark series (1 h) are indicated; * = $P \leq 0.05$, ** = $P \leq 0.01$, *** = $P \leq 0.001$ (Student's *t* test).

Copper has multimodal killing mechanisms, including disruption of bacterial energy generation in the electron transport chain by competing for binding to [Fe–S] clusters[104] and ROS (reactive oxygen species) mediated protein damage and lipid peroxidation.

In the absence of light activation, **Cu1** mediated activity was time-dependent, with <3 log reduction for 1 h incubation (*S. aureus*, *E. coli*) and negligible killing for *P. aeruginosa*. However, photo-activation of **Cu1** at 430 nm, enhanced killing to ≥6 log for *S. aureus* and *E. coli*, but not *P. aeruginosa*, at this much shorter incubation time. This suggests dual activity of **Cu1** under these conditions, with killing mediated by photo-activated singlet oxygen production and from copper-1,10 phenanthroline. To further investigate the activity spectrum, this

Table 1 Summary of antibacterial activity of **Cu1** against ESKAPE pathogens under dark and irradiation conditions

Bacteria	ATCC/NCTC code	Reduction in $\log_{10}$ CFU ml^{-1} for treatment relative to DMSO control[a]			Statistical significance P value[b]
		24 h dark	1 h dark	1 h irradiated	
Gram-positive					
S. aureus	25 923	6.02 ± 0.14	2.85 ± 0.24	6.19 ± 0.05	<0.01**
S. aureus	43 300	2.36 ± 0.16	2.69 ± 0.17	6.17 ± 0.18	<0.001***
E. faecium	7174	1.70 ± 0.09	1.51 ± 0.27	1.09 ± 0.19	>0.05
E. faecium	12 204	<1	<1	<1	>0.05
A. baumannii	19 606	5.80 ± 0.06	3.09 ± 0.65	6.03 ± 0.13	<0.01**
Gram-negative					
E. coli	25 922	5.66 ± 0.16	2.83 ± 0.39	5.96 ± 0.37	<0.001***
K. pneumoniae	9633	<1	<1	<1	>0.05
P. aeruginosa	27 853	2.17 ± 0.27	<1	<1	>0.05
P. aeruginosa	13 437	<1	<1	2.30 ± 0.27	<0.01**
E. cloacae complex	13 405	<1	<1	5.92 ± 0.07	<0.001***

[a] Bacteria incubated with 100 µg ml^{-1} (145.1 µM **Cu1**), values are mean ± SD for three separate assays each conducted in triplicate. [b] For comparison of dark *vs.* irradiated (values in grey shading) using Student's *t* test. ATCC = American Type Culture Collection, NCTC = National Collection of Type Cultures, CFU = colony forming units.

light-activated killing investigation was extended to reference strains and clinical wound isolates of the ESKAPE pathogens. Enhanced activity with irradiation was statistically significant for *S. aureus* ATCC25923 and ATCC44330 (methicillin resistant *S. aureus* (MRSA)), *E. coli* ATCC25922, *A. baumanni* ATCC19606, *E. cloaceae* complex and *P. aeruginosa* ATCC13437. However, for all other pathogens tested, they were either, not susceptible or poorly susceptible to **Cu1** (*e.g.*, *E. faecium* ATCC12204, *P. aeruginosa* ATCC27853) under these conditions, or enhanced activity was observed with light, but it was not statistically significant (Fig. 10 and Table 1). A similar spectrum was observed for clinical isolates recovered from infections, in which irradiation resulted in enhanced activity towards *S. aureus*, including MRSA and *E. coli*. Notably, the *P. aeruginosa* clinical isolates did not show enhanced activity with irradiation, compared to the reference strain (Fig. S15†). A direct comparison of bactericidal activity achieved with **Cu1** relative to antibiotics was precluded on the basis of the wide range of bacterial species investigated including AMR strains, along with the challenge in selecting appropriate comparator antibiotics and assay conditions relevant to topical applications. Nonetheless, some cautious comparisons are possible based on our previous studies and with the caveat that antibiotic susceptibility testing is usually based on Minimum Inhibitory Concentration (MIC). A recent study by Connolly *et al.*, 2024 reported MICs for ciprofloxacin, a broad-spectrum antibiotic, against ESKAPE pathogens ranging from 0.048µM to 12.5 µM.[105] By comparison, the **Cu1** MICs of ESKAPE pathogens (albeit different strains) tested in the present study using the same methodology, ranged from 6.25–200µM (ESI Table S1†).

Copper complexes have unique redox properties that distinguish them from similar complexes with platinum or palladium.[106] This redox activity, is considered crucial for the ability of coordination complexes to mediate DNA cleavage.[107] However, this nuclease activity is not intrinsic and requires the presence of exogenous reagents, such as ascorbate, thiols, and hydrogen peroxide to generate the reactive species responsible for inducing DNA strand scission.[106,108,109] In bacterial systems, the required reducing environment is typically provided by low molecular mass thiols, which are abundant within the bacterial cytoplasm, maintaining it in a strongly reducing state. The specific thiol that delivers this role varies between different types of bacteria. In most Gram-negative bacteria, glutathione serves as the primary low molecular mass thiol, contributing to the maintenance of the cytoplasmic reducing environment. Conversely, in several Gram-positive bacteria, including *S. aureus*, bacillithiol assumes this critical function. Bacillithiol is structurally distinct from glutathione but serves a similar role in sustaining the redox balance within these bacterial cells.[106,110] The interplay between the copper complex, the exogenous reagents, and the bacterial thiols is essential for understanding the mechanism of DNA cleavage. Even without irradiation, differences in capability of bacteria to generate damaging ROS species in response to **Cu1** may partly explain the variations in killing activity across strains (Fig. 12).

One of our initial hypotheses was that the Cu(II) compounds bind to extracellular DNA. Extracellular DNA (eDNA) is known to be a significant component of the extracellular matrix (ECM) in biofilms, which are complex communities of microorganisms adhering to surfaces and encased within a self-produced matrix. The presence of eDNA in the ECM plays a crucial role in the structural integrity and stability of biofilms. This structural role is critical because biofilms provide a protective environment for bacterial communities, making them more resistant to antibiotics and the host immune response. Research has demonstrated that disrupting eDNA can lead to a significant reduction in biofilm biomass. For instance, treatment with DNase, an enzyme that degrades DNA, has been shown to substantially reduce the biomass of

biofilms formed by *S. aureus* and other bacterial species. This reduction occurs because the degradation of eDNA weakens the biofilm structure, making it more susceptible to external forces and antimicrobial agents. In the context of our hypothesis, if Cu(II) compounds bind to eDNA, they could potentially interfere with the integrity of the biofilm matrix in a manner similar to DNase treatment. This interaction could disrupt the biofilm structure, reducing its biomass and making the bacterial communities more vulnerable. Therefore, understanding the binding properties of Cu(II) compounds to eDNA could provide valuable insights into novel strategies for biofilm control and the development of new antimicrobial treatments.[111–117]

Photoactive killing in hydrogels

Exploiting novel antimicrobials for applications in wound treatment or surgery will require their formulation in appropriate matrices in which their antimicrobial activity is maintained. Hydrogel preparations of **Cu1** (145.1 µM) were used to further investigate killing of three bacteria that are among those most frequently associated with wound infections. When incorporated into a hydrogel, **Cu1** retained bactericidal activity without light activation of 5–6 log reduction in CFU ml^{-1} over 24 h (*S. aureus* 5.39 log, *P. aeruginosa* 5.48 log, *A. baumannii* 6.23 log) (Fig. 11). This activity was lower for 1 h incubation but could be enhanced by irradiation, to reach 5–6 log killing across the strains tested (*S. aureus* 2.38 and 5.66 log for dark and irradiated respectively, *P. aeruginosa* 0 *vs.* 5.97 log,

A. baumannii 2.22 *vs.* 5.19 log). The high activity across these bacteria, which was similarly potent for 24 h treatment with **Cu1** impregnated hydrogel alone and for 1 h with the irradiation of the **Cu1** hydrogel is encouraging. This provides the potential for flexibility in clinical practice. For example, in surgical applications, photosensitive antimicrobial hydrogels may be beneficial for skin decolonisation if applied in advance with flexible light activation at the wound site, immediately pre- or post-surgery. This approach has shown positive results for MRSA decolonisation using methylene blue aPDT for nasal decolonisation and chlorhexidine wipes for skin decolonisation, with a significant reduction in surgical site infection among patients in the treatment group compared to controls.[118] The finding that the hydrogel preparations of **Cu1** significantly improved the anti-pseudomonal activity, compared to activity in PBS was unexpected. However, the hydrogel matrix may enhance photodynamic performance due to several factors including prevention of PS aggregation, enhanced stability and enhanced oxygen diffusion. A recent systematic review of PDT delivered using hydrogels for treatment of *S. aureus* infections concluded that this delivery system can enhance PDT efficiency.[119]

Cytotoxicity studies

HaCaT cell viability was determined following exposure to **Cu1** and **L1** for 24 h. The test was performed based on the metabolic activity of the cells using the MTT assay. The IC$_{50}$ value (defined as the concentration at which half the maximum inhi-
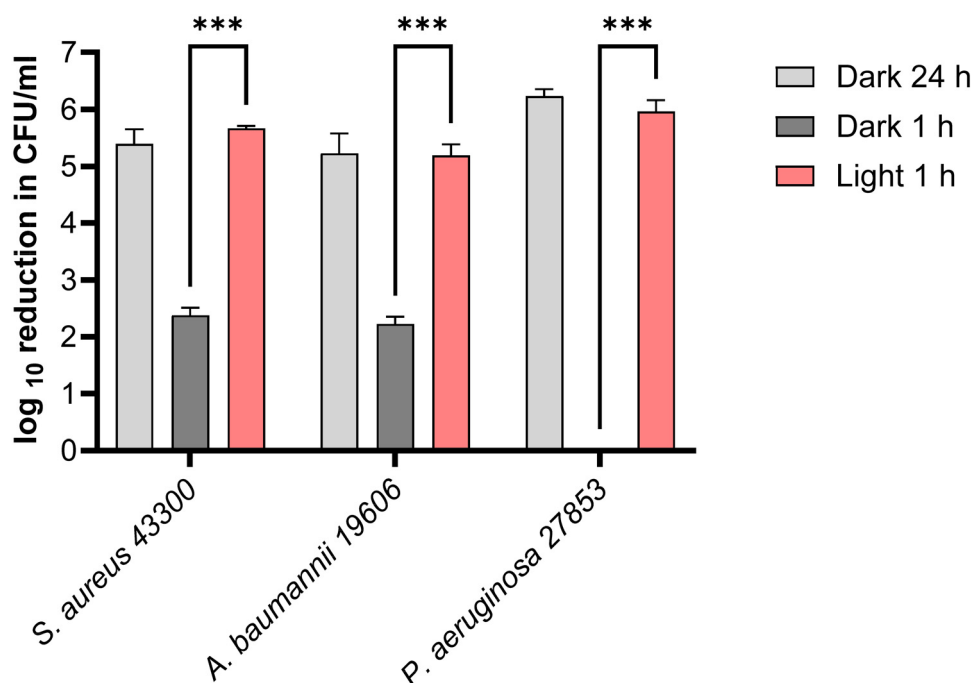

Fig. 11 Bactericidal activity of NDI-Cu (**Cu1**) in hydrogel. **Cu1** in Pluronic F127® hydrogel (100 µg ml^{-1}, 145.1 µM) against *S. aureus* ATCC 44330, *P. aeruginosa* ATCC 27853, and *A. baumannii* ATCC 19606 in the dark for 24 h or for 1 h with and without irradiation. For each data set, CFU ml^{-1} from hydrogels containing **Cu1** (treated), were subtracted from CFU ml^{-1} from hydrogels containing 10% DMSO only (control) and presented as the log difference. Data are the mean $\pm$ SEM for 3 experiments. *** = $P \leq 0.001$.
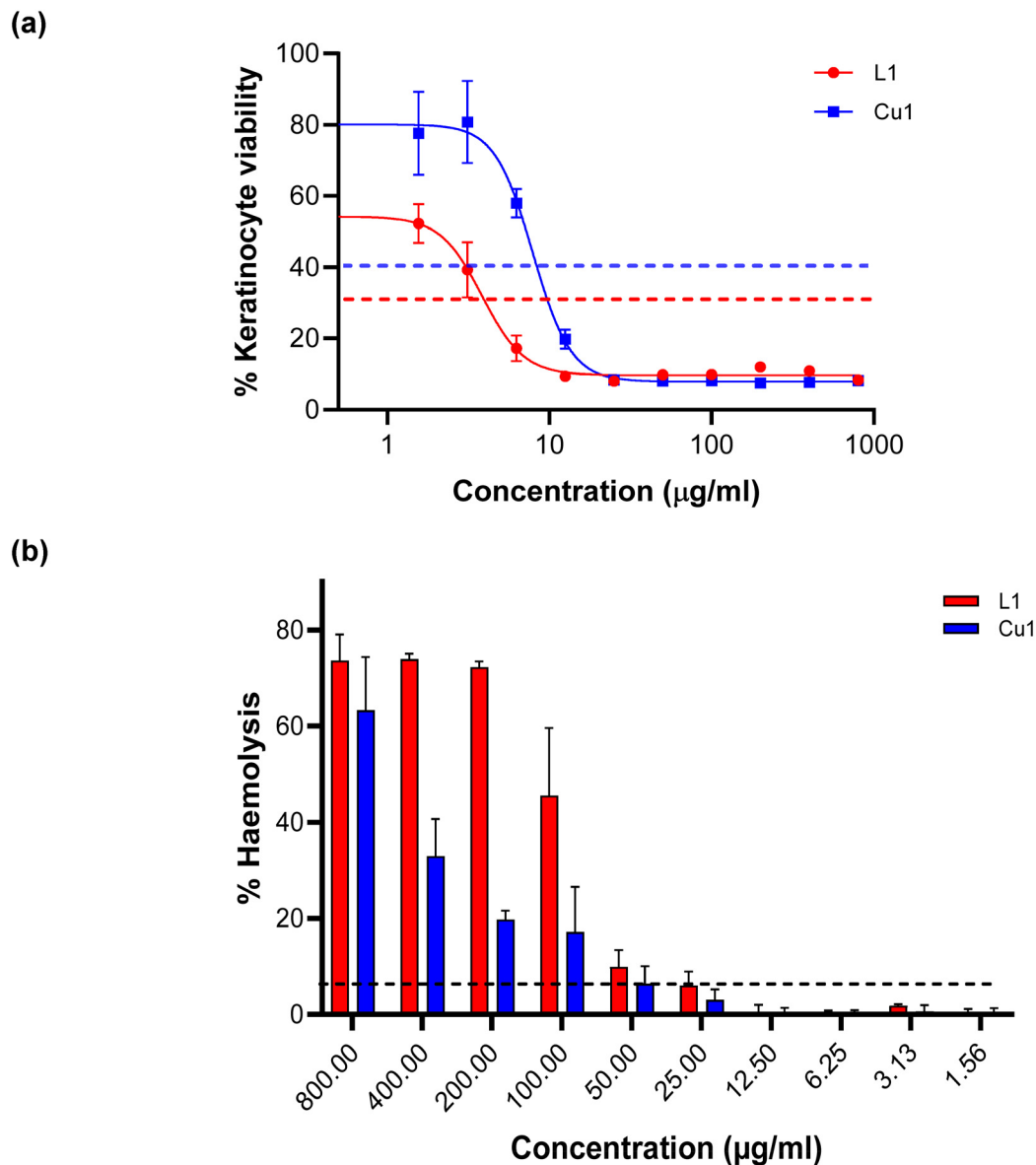
Fig. 12 Biocompatibility testing of **L1** and **Cu1**. HaCaT cells were seeded in 96-well plates and incubated until a confluent monolayer was formed. Cells were treated with decreasing concentrations of **L1** and **Cu1** (800 to 1.56 µg ml^{-1}) and incubated for 24 h. Cell viability after treatment was determined by MTT assay, dashed line indicates half maximal killing, X axis is a log scale (a). Percentage hemolysis of healthy human erythrocytes exposed to 800–1.56 µg ml^{-1} **L1** and **Cu1** for 24 h, dashed line indicated 5% haemolysis (b). Values shown are mean ± SEM for assays carried out three times (each in at least triplicate).

bition of cell metabolic activity occurs) of 8.64 µg ml^{-1} (12.5 µM) (**Cu1**) and 4.64 µg ml^{-1} (8.34 µM) (**L1**) were determined by interpolation of the dose–response curve (Fig. 12a). As shown in Fig. 12b, biocompatibility was further characterized using hemolysis assays that were performed on freshly collected healthy human erythrocytes. At a concentration of 100 µg ml^{-1} at which NDI-Cu (**Cu1**) showed the best antibacterial activity, there was a significant difference in hemolysis induced by **Cu1** 17.12% compared to **L1** 45.52%. The minimal hemolytic concentration, defined as the lowest concentration causing up to 5% hemolysis (MHC 5%) for **L1** was obtained at 12.5 µg ml^{-1} (22.5 µM, 0.32%) while for **Cu1** it was obtained at

25 µg ml^{-1} (36.3 µM, 3.05%). This indicates somewhat improved biocompatibility of **Cu1** compared to **L1**. Nonetheless, the NDI component of the molecule is likely contributing to haemolysis and cytotoxicity in this case. Naphthalene-derived compounds, such as naphthalimide and 1,4,5,8-naphthalenetetracarboxylic diimide, have been extensively investigated for their roles as intercalative agents and potential anticancer therapeutics. Notable representatives of the NI class, including mitonafide and amonafide, showed promising anticancer effects; however, did not pass phase II because of their toxicity.[54] Specific studies on the toxicity of NDIs in HaCaT cells or human erythrocytes are limited.

Nevertheless, given the strong affinity of NDIs for nucleic acids and their capacity to generate ROS, there is concern that NDIs may exert toxic effects, particularly at high doses or under conditions conducive to ROS formation. HaCaT cells, which serve as models for human keratinocytes, are potentially susceptible to oxidative damage from NDIs, especially during photodynamic treatments. Thus, while NDIs offer potential in diagnostic and therapeutic applications, their cytotoxicity under certain conditions underscores the need for careful assessment in biological and clinical use. For technical and resource reasons, potential cytotoxic effects associated with photoactivation could not be tested reliably, which is a study limitation.

Conclusion

A novel copper(II) naphthalenediimide-phenanthroline complex, **Cu1** was synthesised and the photophysical properties determined, in addition to evaluating DNA/BSA binding, cytotoxic properties, and antimicrobial activity. The introduction of naphthalene moieties into inorganic complexes has been demonstrated to be an effective strategy for enhancing the photophysical properties of various systems.[60,72,120] In the case of the **Cu1**, incorporating naphthalene diimide allows for the formation of a long-lived excited state with a lifetime of 270 nanoseconds, without the need for sterically hindering ligands to shield the metal centre. Furthermore, the unique spectral signature of NDI, observable in both the infrared (IR) region and the excited state, makes it a desirable ligand for further studies, such as time-resolved infrared (TRIR) spectroscopy,[121] to explore its excited-state pathways and to investigate the complex's interactions with DNA.

Cu1 exhibited a strong interaction with DNA, as demonstrated by various spectroscopic techniques. Its binding affinity was significantly higher than that of **L1**, suggesting that **Cu1** binds more effectively—likely through intercalation—which may lead to structural alterations in the DNA or interference with replication. Both **Cu1** and **L1** also showed the ability to bind to bovine serum albumin (BSA). Fluorescence quenching studies revealed that **Cu1** (9.29×10^6) had a higher binding constant to BSA than **L1** (8.86×10^6), indicating a stronger affinity for protein binding as well. When comparing **Cu1** to other copper(II) complexes containing only 1,10-phenanthroline ligands, it is evident that the inclusion of the naphthalenediimide moiety significantly enhances the binding dynamics. The increased π–π stacking capability and hydrophobic interactions provided by the naphthalenediimide group are not present in complexes with solely 1,10-phenanthroline, which may explain the observed differences in binding constants. This suggests that the design and synthesis of metal complexes incorporating such moieties could be a viable strategy for enhancing binding interactions with biological molecules.

The antimicrobial tests revealed that the **Cu1** exhibited enhanced activity against a range of bacterial strains compared to **L1**. This increased efficacy is likely due to the synergistic effects of the copper ion, which can disrupt microbial cell membranes and interfere with enzyme functions, in addition to the intrinsic properties of the ligand **L1**.

Research indicates that incorporating copper ions into hydrogels significantly enhances their antibacterial effectiveness. This effect arises from both the hydrogel's structural properties and the controlled release of copper ions, which are well-documented for their ability to disrupt bacterial cell membranes and interfere with metabolic processes, resulting in broad-spectrum antibacterial action. Embedding copper within a hydrogel matrix further amplifies its effects by enabling sustained, gradual ion release, making it a promising approach for applications such as wound healing and infection prevention. In a study by Li *et al.*, a copper–silica nanoparticle-infused hydrogel was developed that leverages near-infrared (NIR) light to activate copper ions, leading to notable antibacterial efficacy against *E. coli* and *S. aureus*. This mechanism facilitates a prolonged ion release profile, crucial for maintaining antibacterial potency over time and particularly valuable for wound care and medical coatings.[122] Similarly, Ivanova *et al.* reported that copper nanoparticles embedded in hydrogels exhibit consistent antimicrobial action that may counteract the rise of bacterial resistance, proving effective against resistant strains such as MRSA. The hydrogel matrix plays an essential role in stabilizing the copper nanoparticles, potentially lowering cytotoxicity and allowing for targeted antimicrobial activity in medical contexts.[123]

Overall, the results of this study highlight the potential of the **Cu1** as a multifaceted bioactive agent with promising applications in medical and pharmaceutical fields. The built-in photodynamic properties of **Cu1** can shorten the time required for its antimicrobial activity. While poor biocompatibility properties in solution, most likely due to the NDI component, requires further compounds optimisation, its strong DNA and BSA interactions suggest possible uses in targeted drug delivery systems. Importantly, confirmation of potent antimicrobial activity in hydrogel formulations is further evidence of its potential for pharmaceutical applications.

Conflicts of interest

There are no conflicts to declare.

Data availability

All experimental data supporting the findings of this study are available within the article and its ESI.† Raw spectroscopic data generated during the study are available from the corresponding author upon reasonable request.

Acknowledgements

References

1 F. Prestinaci, P. Pezzotti and A. Pantosti, *Pathog. Global Health*, 2015, **109**, 309–318.

2 C. L. Ventola, *Pharm. Ther.*, 2015, **40**(4), 277–283.

3 M. S. Butler and D. L. Paterson, *J. Antibiot.*, 2020, **73**(6), 329–364.

4 U. Theuretzbacher, K. Bush, S. Harbarth, M. Paul, J. H. Rex, E. Tacconelli and G. E. Thwaites, *Nat. Rev. Microbiol.*, 2020, **18**(5), 286–298.

5 U. Theuretzbacher, K. Outterson, A. Engel and A. Karlén, *Nat. Rev. Microbiol.*, 2020, **18**(5), 275–285.

6 H. W. Boucher, G. H. Talbot, J. S. Bradley, J. E. Edwards, D. Gilbert, L. B. Rice, M. Scheld, B. Spellberg and J. Bartlett, *Clin. Infect. Dis.*, 2009, **48**(1), 1–12.

7 World Health Organization, *Global Priority List of Antibiotic-Resistant Bacteria to Guide Research, Discovery, and Development of New Antibiotics*, World Health Organization, 2017.

8 K. H. Thompson and C. Orvig, *Dalton Trans.*, 2006, 761–764.

9 J. K. Barton, *Science*, 1986, **233**, 727–734.

10 D. R. Mcmillin and K. M. Mcnett, *Chem. Rev.*, 1998, **98**, 1201–1219.

11 J. A. Cowan, *Curr. Opin. Chem. Biol.*, 2001, **5**, 634–642.

12 S. Dhar and A. R. Chakravarty, *Inorg. Chem.*, 2003, **42**, 2483–2485.

13 E. I. Solomon, D. E. Heppner, E. M. Johnston, J. W. Ginsbach, J. Cirera, M. Qayyum, M. T. Kieber-Emmons, C. H. Kjaergaard, R. G. Hadt and L. Tian, *Chem. Rev.*, 2014, **114**, 3659–3853.

14 S. Rajalakshmi, T. Weyhermüller, A. J. Freddy, H. R. Vasanthi and B. U. Nair, *Eur. J. Med. Chem.*, 2011, **46**, 608–617.

15 P. Jaividhya, R. Dhivya, M. A. Akbarsha and M. Palaniandavar, *J. Inorg. Biochem.*, 2012, **114**, 94–105.

16 C. Santini, M. Pellei, V. Gandin, M. Porchia, F. Tisato and C. Marzano, *Chem. Rev.*, 2014, **114**, 815–862.

17 C. Rajarajeswari, M. Ganeshpandian and M. Palaniandavar, *J. Inorg. Biochem.*, 2014, **140**, 255–268.

18 B. Zhang, X. Lu, G. Wang, W. Zhang, S. Xia and Y. Chen, *J. Inorg. Biochem.*, 2014, **140**, 213–218.

19 I. Correia, S. Roy, C. P. Matos, S. Borovic, I. Butenko, I. Cavaco, F. Marques, J. Lorenzo, A. Rodríguez, V. Moreno and J. C. Pessoa, *J. Inorg. Biochem.*, 2015, **147**, 134–146.

20 M. Liu, H. Yang, D. Li, Q. Yao, H. Wang, Z. Zhang and J. Dou, *Inorg. Chim. Acta*, 2021, **522**, 120384.

21 R. M. Gandra, P. M. Carron, M. F. Fernandes, L. S. Ramos, T. P. A. C. Aor, M. H. Branquinha, M. McCann, M. Devereux and A. L. S. Santos, *Front. Microbiol.*, 2017, **8**, 1–11.

22 F. Gomes da Silva Dantas, A. Araújo de Almeida-Apolonio, R. Pires de Araújo, L. Regiane Vizolli Favarin, P. Fukuda de Castilho, F. de Oliveira Galvão, T. Inez Estivalet Svidzinski, G. Antonio Casagrande and K. Mari Pires de Oliveira, *Molecules*, 2018, **23**, 1–14.

23 J. A. de Azevedo-França, L. P. Borba-Santos, G. de Almeida Pimentel, C. H. J. Franco, C. Souza, J. de Almeida Celestino, E. F. de Menezes, N. P. dos Santos, E. G. Vieira, A. M. D. C. Ferreira, W. de Souza, S. Rozental and M. Navarro, *J. Inorg. Biochem.*, 2021, **219**, 111401.

24 K. Bajaj, R. M. Buchanan and C. A. Grapperhaus, *J. Inorg. Biochem.*, 2021, **225**, 111620.

25 R. Rao, A. K. Patra and P. R. Chetana, *Polyhedron*, 2007, **26**, 5331–5338.

26 S. Rajalakshmi, A. Fathima, J. R. Rao and B. U. Nair, *RSC Adv.*, 2014, **4**, 32004–32012.

27 N. S. Ng, M. J. Wu and J. R. Aldrich-Wright, *J. Inorg. Biochem.*, 2018, **180**, 61–68.

28 J. D. Ranford, P. J. Sadler and D. A. Tocher, *J. Chem. Soc., Dalton Trans.*, 1993, 3393–3399.

29 S. Dorotíková, J. Kozísková, M. Malcek, K. Jomova, P. Herich, K. Plevova, K. Briestenska, A. Chalupkova, J. Mistríková, V. Milata, D. Dvoranova and L. Bucinský, *J. Inorg. Biochem.*, 2015, **150**, 160–173.

30 J. Joseph, K. Nagashri and G. B. Janaki, *Eur. J. Med. Chem.*, 2012, **49**, 151–163.

31 A. R. Barbosa, K. R. Caleffi-Ferracioli, C. Q. F. Leite, J. C. García-Ramos, Y. Toledano-Magana, L. Ruiz-Azuara, V. L. D. Siqueira, F. R. Pavan and R. F. Cardoso, *Chemotherapy*, 2016, **61**, 249–255.

32 G. S. S. Firmino, M. V. N. de Souza, C. Pessoa, M. C. S. Lourenco, J. A. L. C. Resende and J. A. Lessa, *BioMetals*, 2016, **29**, 953–963.

33 G. S. Hegde, S. S. Bhat, S. P. Netalkar, P. L. Hegde, A. Kotian, R. J. Butcher and V. K. Revankar, *Inorg. Chim. Acta*, 2021, **522**, 120352.

34 N. H. Gokhale, K. Shirisha, S. B. Padhye, S. L. Croft, H. D. Kendrick and V. Mckee, *Bioorg. Med. Chem. Lett.*, 2006, **16**, 430–432.

35 T. J. Hubin, P. N. A. Amoyaw, K. D. Roewe, N. C. Simpson, R. D. Maples, T. N. Carder Freeman, A. N. Cain, J. G. Le, S. J. Archibald, S. I. Khan, B. L. Tekwani and M. O. F. Khan, *Bioorg. Med. Chem.*, 2014, **22**, 3239–3244.

36 T. Kiran, V. G. Prasanth, M. M. Balamurali, C. S. Vasavi, P. Munusami, K. I. Sathiyanarayanan and M. Pathak, *Inorg. Chim. Acta*, 2015, **433**, 26–34.

37 J. J. Martínez Medina, M. S. Islas, L. L. Lopez Tevez, E. G. Ferrer, N. B. Okulik and P. A. M. Williams, *J. Mol. Struct.*, 2014, **1058**, 298–307.

38 N. S. Ng, M. J. Wu, C. E. Jones and J. R. Aldrich-Wright, *J. Inorg. Biochem.*, 2016, **162**, 62–72.

39 P. Sureshbabu, B. Varghese, E. Sujitha and S. Sabiah, *Inorg. Chim. Acta*, 2022, **536**, 120898.

40 Y. Cheng, X. Han, H. Ouyanga and Y. Rao, *Chem. Commun.*, 2012, **48**, 2906–2908.

41 J. Bolger, A. Gourdon, E. Ishow and J.-P. Launay, *Inorg. Chem.*, 1996, **35**(10), 2937–2944.

42 H. Xu, K.-C. Zheng, Y. Chen, Y.-Z. Li, L.-J. Lin, H. Li, P.-X. Zhang and L.-N. Ji, *Dalton Trans.*, 2003, **11**, 2260–2268.

43 S. Rothman and W. C. Yang, *Am. J. Physiol.*, 1964, **206**, 283–288.

44 I. Druta, C. Cuciac, R. Danac, E. Avram, A. Rotaru and G. Drochioiu, *Pak. J. Appl. Sci.*, 2002, **2**(2), 145–149.

45 N. Singh, D. Pagariya, S. Jain, S. Naik and N. Kishore, *J. Biomol. Struct. Dyn.*, 2017, **36**(9), 2449–2462.

46 S. K. Tarai, S. Mandal, A. Tarai, I. Som, A. Pan, A. Bagchi, A. Biswas and S. Ch. Moi, *Appl. Organomet. Chem.*, 2023, **37**, e7164.

47 P. Nunes, I. Correia, F. Marques, A. P. Matos, M. M. C. dos Santos, C. G. Azevedo, J.-L. Capelo, H. M. Santos, S. Gama, T. Pinheiro, I. Cavaco and J. C. Pessoa, *Inorg. Chem.*, 2020, **59**(13), 9116–9134.

48 O. Zelenko, J. Gallagher and D. S. Sigman, *Angew. Chem., Int. Ed. Engl.*, 1997, **36**, 2776–2778.

49 A. Robertazzi, A. V. Vargiu, A. Magistrato, P. Ruggerone, P. Carloni, P. de Hoog and J. Reedijk, *J. Phys. Chem. B*, 2009, **113**(31), 10881–10890.

50 A. T. Gordon, O. O. Abosede, S. Ntsimango, S. van Vuuren, E. C. Hosten and A. S. Ogunlaja, *Inorg. Chim. Acta*, 2020, **510**, 119744.

51 S. Min, L. Cao, T. C. Pham, V. K. T. Nguyen, D. S. Kim, S. G. Lee and S. Lee, *Sens. Actuators, B*, 2025, **433**, 137526.

52 O. Krupka and P. Hudhomme, *Int. J. Mol. Sci.*, 2023, **24**, 6308.

53 V. Pirota, E. Salvati, C. Risoldi, F. Manoli, A. Rizzo, P. Zizza, A. Biroccio, M. Freccero, I. Manet and F. Doria, *Biomolecules*, 2025, **15**, 311.

54 V. Tumiatti, A. Milelli, A. Minarini, M. Micco, A. G. Campani, L. Roncuzzi, D. Baiocchi, J. Marinello, G. Capranico, M. Zini, C. Stefanelli and C. Melchiorre, *J. Med. Chem.*, 2009, **52**, 7873–7877.

55 C. Marchetti, A. Minarini, V. Tumiatti, F. Moraca, L. Parrotta, S. Alcaro, R. Rigo, C. Sissi, M. Gunaratnam, S. A. Ohnmacht, S. Neidle and A. Milelli, *Bioorg. Med. Chem.*, 2015, **23**, 3819–3830.

56 X. Xu, S. Wang, Y. Chang, C. Ge, X. Li, Y. Feng, S. Xie, C. Wang, F. Dai and W. Luo, *Med. Chem. Commun.*, 2018, **9**, 1377–1385.

57 R. Cebrián, E. Belmonte-Reche, V. Pirota, A. de Jong, J. Carlos Morales, M. Freccero, F. Doria and O. P. Kuipers, *J. Med. Chem.*, 2022, **65**(6), 4752–4766.

58 N. M. Shavaleev, E. S. Davies, H. Adams, J. Best and J. A. Weinstein, *Inorg. Chem.*, 2008, **47**, 1532–1547.

59 I. V. Sazanovich, M. A. H. Alamiry, J. Best, R. D. Bennett, O. V. Bouganov, E. S. Davies, V. P. Grivin, A. J. H. M. Meijer, V. F. Plyusnin, K. L. Ronayne, A. H. Shelton, S. A. Tikhomirov, M. Towrie and J. A. Weinstein, *Inorg. Chem.*, 2008, **47**, 10432–10445.

60 K. Sharun, S. S. Nair, S. A. Banu, *et al.*, *J. Pure Appl. Microbiol.*, 2023, **17**(2), 1231–1237.

61 M. E. Reichmann, S. A. Rice and P. A. Thomas, *J. Am. Chem. Soc.*, 1954, **76**, 3047.

62 P. Krishnamoorthy, P. Sathyadevi, R. R. Butorac, A. H. Cowley, N. S. P. Bhuvaneshc and N. Dharmaraj, *Dalton Trans.*, 2012, **41**, 4423–4436.

63 J. R. Lakowicz and G. Weber, *Biochemistry*, 1973, **12**, 4161.

64 M. Kumar, G. Kumar and D. T. Masram, *New J. Chem.*, 2020, **44**, 8595–8613.

65 A. Blacha-Grzechnik, A. Drewniak, K. Z. Walczak, M. Szindler and P. Ledwon, *J. Photochem. Photobiol., A*, 2020, **388**, 112161.

66 G.-P. Zu, J.-J. Wang, Y. Zhang, W.-B. Chen, Y.-Z. Shi, S.-W. Guo and X.-R. Wang, *ChemistrySelect*, 2019, **4**, 863–867.

67 A. Doherty, R. Murphy, A. Heise, F. Fitzpatrick and D. Fitzgerald-Hughes, *J. Med. Microbiol.*, 2024, **73**(9), 001886.

68 A. A. Miles, S. S. Misra and J. O. Irwin, *J. Hyg.*, 1938, **38**(6), 732–749.

69 M. Zapotoczna, É. Forde, S. Hogan, H. Humphreys, J. P. O'Gara, D. Fitzgerald-Hughes, M. Devocelle and E. O'Neill, *J. Infect. Dis.*, 2017, **215**(6), 975–983.

70 A. Demeter, T. Bérces, L. Biczók, V. Wintgens, P. Valat and J. Kossanyi, *J. Phys. Chem.*, 1996, **100**, 2001–2011.

71 T. C. Barros, S. Brochsztain, V. G. Toscano, P. B. Filho and M. Politi, *J. Photochem. Photobiol., A*, 1997, **111**, 97–104.

72 V. Wintgens, P. Valat, J. Kossanyi, L. Biczok, A. Demeter and T. Bérces, *J. Chem. Soc., Faraday Trans.*, 1994, **90**, 411–421.

73 B. Abraham, S. McMasters, M. A. Mullan and L. A. Kelly, *J. Am. Chem. Soc.*, 2004, **126**, 4293–4300.

74 D. Hayes, L. Kohler, L. X. Chen and K. L. Mulfort, *J. Phys. Chem. Lett.*, 2018, **9**, 2070–2076.

75 B. M. Aveline, S. Matsugo and R. W. Redmond, *J. Am. Chem. Soc.*, 1997, **119**, 11785–11795.

76 S. Green and M. A. Fox, *J. Phys. Chem.*, 1995, **99**, 14752–14757.

77 J. E. Rogers, S. J. Weiss and L. A. Kelly, *J. Am. Chem. Soc.*, 2000, **122**, 427–436.

78 S. A. Tysoe, R. J. Morgan, A. D. Baker and T. C. Strekas, *J. Phys. Chem.*, 1993, **97**, 1707.

79 T. M. Kelly, A. B. Tossi, D. J. McConnell and T. C. A. Strekas, *Nucleic Acids Res.*, 1985, **13**, 6017.

80 J. S. Guerrero, P. C. Sanchez, E. R. Perez, F. V. Garcia, M. E. B. Gomez and L. R. Azuara, *Toxicol. in Vitro*, 2011, **25**, 1376.

81 P. R. Reddy and N. Raju, *Polyhedron*, 2012, **44**(1), 1–10.

82 D. İnci, R. Aydın, Ö. Vatan, D. Yılmaz, H. M. Gençkal, Y. Zorlu and T. Cavaş, *Spectrochim. Acta, Part A*, 2015, **145**, 313–324.

83 V. Pirota, E. Lunghi, A. Benassi, E. Crespan, M. Freccero and F. Doria, *Molecules*, 2021, **26**, 5025.

84 P. Mignon, S. Loverix, J. Steyaert and P. Geerlings, *Nucleic Acids Res.*, 2005, **33**, 1779–1789.

85 J. Lakshmipraba, S. Arunachalam, D. Avinash Gandi and T. Thirunalasundari, *Eur. J. Med. Chem.*, 2011, **46**, 3013–3021.

86 J. Ramesh, S. Sujatha and C. Arunkumar, *RSC Adv.*, 2016, **6**, 63271–63285.

87 N. Varga, V. Hornok, D. Sebők and I. Dékány, Comprehensive study on the structure of the BSA from extended-to aged form in wide (2–12) pH range, *Int. J. Biol. Macromol.*, 2016, **88**, 51–58.

88 N. Zhou and A. Facchetti, *Mater. Today*, 2018, **21**, 377–390.

89 Á. Sánchez-González, N. A. G. Bandeira, I. Ortiz de Luzuriaga, F. F. Martins, S. Elleuchi, K. Jarraya, J. Lanuza, X. Lopez, M. J. Calhorda and A. Gil, *Molecules*, 2021, **26**(16), 4737.

90 S. A. Shaikh, S. S. Bhat, V. Kamat and V. K. Revankar, *J. Mol. Struct.*, 2020, **1205**, 127557.

91 D. İnci, R. Aydın, Ö. Vatan, T. Sevgi, D. Yılmaz, Y. Zorlu, Y. Yerli, B. Çoşut, E. Demirkan and N. Çinkılıç, *J. Biol. Inorg. Chem.*, 2017, **22**, 61–85.

92 Q. Jiao, R. Wang, Y. Jiang and B. Liu, *Chem. Cent. J.*, 2018, **12**(1), 48.

93 Y. Hu, Y. Yang, C. Dai, Y. Liu and X. Xiao, *Biomacromolecules*, 2010, **11**, 106–112.

94 B. Ahmad, S. Parveen and R. H. Khan, *Biomacromolecules*, 2006, **7**, 1350.

95 J. Yang, X.-R. Liu, M.-K. Yu, W.-B. Yang, Z.-W. Yang and S.-S. Zhao, *Polyhedron*, 2020, **187**, 114619.

96 S. Mandal, R. Naskar, A. S. Mondal, B. Beraa and T. K. Mondal, *Dalton Trans.*, 2023, **52**, 5983–5998.

97 A. Abedi, Z. M. Lighvan and S. Nasser Ostad, *Monatsh. Chem.*, 2016, **147**, 1651–1658.

98 N. Singh, D. Pagariya, S. Jain, S. Naik and N. Kishore, *J. Biomol. Struct. Dyn.*, 2017, **36**, 2449–2462.

99 P. Acharya, A. Kuila, U. Pramanik, V. R. Hathwar, P. Brandao, S. Mukherjee, S. Maity, T. Maity, R. Maity and B. C. Samanta, *RSC Adv.*, 2023, **13**, 7632–7644.

100 B. Anupama, A. Aruna, V. Manga, S. Sivan, M. V. Sagar and R. Chandrashekar, *J. Fluoresc.*, 2017, **27**, 953–965.

101 Q. Wang, H. Mao, W. Wang, H. Zhu, L. Dai, Y. Chen and X. Tang, *BioMetals*, 2017, **30**, 575–587.

102 A. L. Pereira, M. A. Vasconcelos, A. L. Andrade, I. M. Martins, A. K. M. Holanda, A. C. S. Gondim, D. P. S. Penha, K. L. Bruno, F. O. N. Silva and E. H. Teixeira, *Curr. Microbiol.*, 2023, **80**(4), 133.

103 T. S. Lobana, S. Indoria, A. K. Jassal, H. Kaur, D. S. Arora and J. P. Jasinski, *Eur. J. Med. Chem.*, 2014, **76**, 145–154.

104 G. Tan, Z. Cheng, Y. Pang, A. P. Landry, J. Li, J. Lu and H. Ding, *Mol. Microbiol.*, 2014, **93**(4), 629–644.

105 J. R. F. B. Connolly, D. Fitzgerald-Hughes, M. Maresca, J. Muldoon and M. Devocelle, *New J. Chem.*, 2024, **48**, 15722–15725.

106 M. L. Beeton, J. R. Aldrich-Wright and A. Bolhuis, *J. Inorg. Biochem.*, 2014, **140**, 167–172.

107 D. S. Sigman, A. Mazumder and D. M. Perrin, *Chem. Rev.*, 1993, **93**, 2295–2316.

108 K. A. Reich, L. E. Marshall, D. R. Graham and D. S. Sigman, *J. Am. Chem. Soc.*, 1981, **103**, 3582–3584.

109 J. M. Vaal, K. Mechant and R. L. Rill, *Nucleic Acids Res.*, 1991, **19**, 3383–3388.

110 G. L. Newton, M. Rawat, J. J. La Clair, V. K. Jothivasan, T. Budiarto, C. J. Hamilton, A. Claiborne, J. D. Helman and R. C. Fahey Nat, *Chem. Biol.*, 2009, **5**, 625–627.

111 H. C. Flemming and J. Wingender, *Nat. Rev. Microbiol.*, 2010, **8**(9), 623–633.

112 C. B. Whitchurch, T. Tolker-Nielsen, P. C. Ragas and J. S. Mattick, *Science*, 2002, **295**(5559), 1487.

113 V. V. Tetz and G. V. Tetz, *DNA Cell Biol.*, 2010, **29**(8), 399–405.

114 J. B. Kaplan and D. H. Fine, *Appl. Environ. Microbiol.*, 2002, **68**(9), 4943–4947.

115 C. E. Santo, D. Quaranta and G. Grass, *MicrobiologyOpen*, 2012, **1**(1), 46–52.

116 J. A. Lemire, J. J. Harrison and R. J. Turner, *Nat. Rev. Microbiol.*, 2013, **11**(6), 371–384.

117 K. C. Rice, E. E. Mann, J. L. Endres, E. C. Weiss, J. E. Cassat, M. S. Smeltzer and K. W. Bayles, *Proc. Natl. Acad. Sci. U. S. A.*, 2007, **104**, 8113–81138.

118 E. Bryce, T. Wong, L. Forrester, B. Masri, D. Jeske, K. Barr, S. Errico and D. Roscoe, *J. Hosp. Infect.*, 2014, **88**(2), 89–95.

119 I. Oliveira-Silva, R. F. Oliveira, D. A. A. P. Oliveira, D. B. Santos, C. H. M. Silva, O. A. Guedes, G. Insalaco and L. V. F. Oliveira, *Gels*, 2024, **10**(10), 635.

120 M. Skaisgirski, X. Guo and O. S. Wenger, *Inorg. Chem.*, 2017, **56**(5), 2432–2439.

121 J. M. Butler, M. W. George, J. R. Schoonover, D. M. Dattelbaum and T. J. Meyer, *Coord. Chem. Rev.*, 2007, **251**, 492–514.

122 M. Li, X. Liu, L. Tan, Z. Cui, X. Yang, Z. Li, Y. Zheng, K. Wai Kwok Yeung, P. K. Chue and S. Wu, *Biomater. Sci.*, 2018, **6**, 2110.

123 I. A. Ivanova, D. S. Daskalova, L. P. Yordanova and E. L. Pavlova, *Processes*, 2024, **12**, 352.